JGR Earth Surface

RESEARCH ARTICLE
10.1029/2023JF007383

Machine Learning Predictions of Vertical Accretion in the Mississippi River Deltaic Plain

Etienne Chenevert[1] and **Douglas A. Edmonds**[1]

[1]Department of Earth and Atmospheric Sciences, Indiana University-Bloomington, Bloomington, IN, USA

Key Points:

- We use a machine learning framework to understand how vertical accretion varies by marsh community and across the Mississippi River Deltaic plain
- We found that large tidal amplitude and flood depth positively affect vertical accretion
- Normalized difference vegetation index is also important in our model because it distinguishes marsh communities in the delta

Correspondence to:
E. Chenevert,
eachenevert@gmail.com

Citation:
Chenevert, E., & Edmonds, D. A. (2024). Machine learning predictions of vertical accretion in the Mississippi River Deltaic plain. *Journal of Geophysical Research: Earth Surface*, *129*, e2023JF007383. https://doi.org/10.1029/2023JF007383

Received 15 AUG 2023
Accepted 20 FEB 2024

Abstract Deltaic landscapes consist of vast wetland systems that rely on sedimentation to maintain their elevation and ecological communities against relative sea-level rise. In the Mississippi River Deltaic plain, rising relative sea level and anthropogenic activities are causing land loss that will continue unless vertical accretion of sediment on the wetland surface is enough to fill the accommodation space. Even though the fate of the Mississippi Deltaic plain is tied directly to vertical accretion, there is not yet a clear understanding of the system-wide controls on this process. Here, we investigate vertical accretion in coastal Louisiana using a data set of 266 stations from the Coastwide Reference Monitoring System (CRMS). Using linear regression models, we analyze vertical accretion in freshwater-intermediate, brackish, and saline marsh communities. Integrating results from these models into a Gaussian Process regression model, we predict controls on vertical accretion rates across the deltaic plain. Consistent with previous studies, our results suggest that tidal amplitude and flood depth are critical controls on vertical accretion. These effects are additive and marshes with high tidal amplitudes and flood depths experience the most vertical accretion. Interestingly, the normalized difference vegetation index is found to be important for predicting vertical accretion, but not because of an increase in biomass production, but because it records unique marsh communities and flooding regimes. This study emphasizes the importance of incorporating marsh specific information into predictive models for the vertical accretion of coastal wetlands and that better predictions of wetland accretion probably require denser observational data.

Plain Language Summary The Mississippi River Deltaic plain (MRDP) is a threatened landscape as the Gulf of Mexico encroaches inland due to relative sea-level rise. To prevent further coastal land loss, enough sediment must be deposited onto the wetland surface to offset the relative sea-level rise. Even though the fate of the MRDP is directly tied to sedimentation, we still do not have a system-wide understanding of what controls this process. We used 266 stations that recorded numerous environmental variables from the Coastwide Reference Monitoring System to investigate the controls on sedimentation. Using a machine learning framework, we find that tidal amplitude and flood depth have additive effects that positively affect sedimentation rates. Interestingly, the normalized difference vegetation index is found to be important for predicting sedimentation, but not due to an increase in biomass production, but because it records unique wetland communities and flooding regimes. This study emphasizes the importance of building predictive models for sedimentation that consider specific information about different wetland types.

1. Introduction

The coastal wetlands of the Mississippi River Deltaic Plain (MRDP) contain diverse flora and fauna, and constitute roughly 37% of the wetlands in the United States (Baustian et al., 2021; Couvillion et al., 2011). Beyond their ecological importance, these wetlands sequester atmospheric carbon and protect communities against hurricanes and tropical storms (Barbier et al., 2013; Cahoon et al., 2006; Turner et al., 2006) as well as provide economically important landscapes for tourism and fisheries. Whether these wetlands survive or disappear in the face of rising relative sea-level comes down to sediment mass balance (Blum & Roberts, 2009; Brown et al., 2017; Edmonds et al., 2023; Sanks et al., 2020; White et al., 2019). The MRDP is currently experiencing a sediment deficit, which means there is not enough sediment input to the wetland surfaces to raise their elevations at the rate of relative sea level rise, and this results in land loss.

The sediment deficit on the MRDP may have been caused by humans because they have interfered with the sediment mass balance and disrupted the normal pathways of sediment transport. For example, dam construction has reduced sediment concentration in the Mississippi River by ~75% since 1890 (Blum & Roberts, 2009; Meade

& Moody, 2009; Tweel & Turner, 2012; K. Xu et al., 2019). Levee construction in the delta impedes the pathways of floodwaters that would normally deliver sediment to the wetlands. Subsurface fluid extraction may be significantly increasing relative sea level (Day et al., 2020; Kolker et al., 2011). These three major causes can explain the land loss in the Barataria Basin, a part of the delta (Edmonds et al., 2023). Despite these human-induced disruptions to the sediment transport pathways, land loss in the delta has significantly slowed down during the last 20 years (Blum et al., 2023; Couvillion et al., 2017; Edmonds et al., 2023; Roy et al., 2020; Sanks et al., 2020). Sanks et al. (2020) showed that in some parts of the delta, sedimentation may be balancing relative sea level rise, though significant uncertainty remains because variability in sedimentation is substantial (Bianchette et al., 2015; Lane et al., 2020). Accurate predictions of land loss on the MRDP strongly depend on understanding the variables that control vertical accretion and its variability.

In a broad sense, wetland sedimentation or vertical accretion can be derived from organic or inorganic sediment. The former is associated with both the above- and below-ground production of plant material. The aboveground biomass contributing to organic accretion consists of the in situ dying of vegetation and leaf litter, while the belowground biomass accumulation consists of the production of root structures (McKee, 2011; Turner et al., 2002, 2004; Twilley et al., 2019). Allochthonous organic sediment is also deposited onto the wetland surface via flood waters (Mariotti et al., 2020). For organic sediment to positively contribute to surface elevation, it must be preserved instead of decomposing. Microbial activity increases the degradation of organics in the soil (Hayes et al., 2021); however, anaerobic conditions during inundation can increase preservation by slowing decomposition rates (Hayes et al., 2021; Reddy & DeLaune, 2008). Differences in both decomposition rates and burial rates vary along salinity gradients in tidal wetlands, where faster decomposition rates and slower burial rates are found in more saline wetlands (Nyman et al., 1995; Weston et al., 2011). Furthermore, saline intrusions have been shown to negatively impact plant growth rates and productivity while enhancing the decomposition of organic materials (Baustian et al., 2017; Cormier et al., 2013; Curcó et al., 2002; Janousek & Mayo, 2013; Solohin et al., 2020; Stagg et al., 2018; Weston et al., 2011; Williams & Rosenheim, 2015). Both effects of salinity reduce the amount of preserved organic sediment, which manifests as higher soil bulk density with more inorganics moving toward the coastline (Sanks et al., 2020).

Inorganic sediment in the delta is derived from the creation, breakdown, and transport of geologic material in the Mississippi watershed, which is eventually deposited along the deltaic plain or offshore (Blum & Roberts, 2012; Falcini et al., 2012). Much of the vertical accretion of this sediment occurs from episodic floods via the over-topping of nearby rivers into the adjacent floodplain (J. M. Coleman, 1988; Shen et al., 2015). The adjacent floodplain can have high shallow subsidence rates and ample accommodation space that readily preserve de-posits. Shen et al. (2015) found that, on the MRDP, aggradation is episodic with vertical accretion rates from 1 to 4 cm/year that can persist for centuries. Inundation and sediment resuspension from tides, storm surges, and wave energy have also been shown to accrete wetland surfaces (Bianchette et al., 2015; Cahoon et al., 2006; Cortese & Fagherazzi, 2022; Turner et al., 2006). While floods deliver a substantial amount of inorganic sediment (Smith et al., 2015; Turner et al., 2006), they also induce erosion (Törnqvist et al., 2007), which is not always accounted for in mass balance estimates.

During tidal flooding, sediment from the ocean can also be delivered to wetland surfaces. The provenance of oceanic-derived sediment is not always clear, but at least in one well-documented case, the sediment discharged out of the Mississippi Delta river mouths was transported back on shore (Falcini et al., 2012). When the river mouth sediment plume mixes with the coastal waters of the basin, it can become more diffuse, losing energy, and thus promoting deposition in the nearby delta (J. M. Coleman, 1988; Falcini et al., 2012). This can result in both the progradation of the delta and the redeposition of sediment onto the wetland surfaces. On the other hand, if the coastal currents and wave regimes are not sufficient to diffuse the jet, or if the conditions create density currents (Lamb & Mohrig, 2009), sediment may be deposited far offshore (Falcini et al., 2012).

To complicate matters, organic and inorganic sedimentation are not independent variables. For example, flooding delivers inorganic sediment and influences vegetation growth. Inundation, frequency, and depth both affect vegetation species and their development, leading to spatially coupled ecological and flooding regimes (Evers et al., 1998; Hiatt et al., 2019; Kirwan & Guntenspergen, 2012; Visser et al., 1999). Depending on the vegetation type and density, vegetation can enhance or diminish inorganic sediment deposition (Ensign et al., 2014; Mudd et al., 2010; Nardin & Edmonds, 2014; Y. Xu et al., 2022). This represents a physical and biological coupling between flooding and vegetation growth with sediment deposition. However, there are few comprehensive

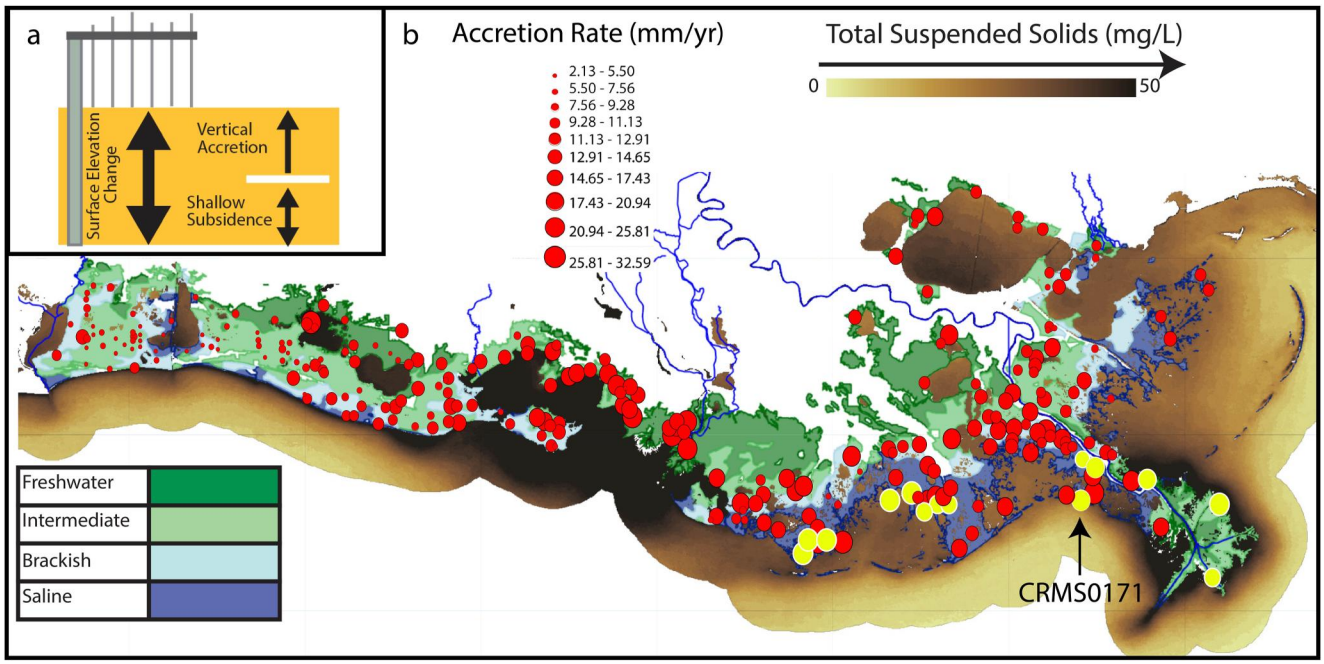

Figure 1. (a) Schematic of the RSET table recording vertical accretion. (b) Map of coastal Louisiana depicting the different marsh communities, total suspended sediment estimations, river vectors (blue lines) from the Global River Width from Landsat data set, non-land pixels corresponding to the 90% water occurrence mask, and average accretion rates at each 266 Coastwide Reference Monitoring System (CRMS) stations used in the machine learning model. The circles highlighted in yellow represent CRMS stations that experience both tidal amplitudes and flood depths that exceed the 75th percentile of their respective distributions. The CRMS0171 station is the station used in the results section to explain SHapley Additive exPlanations (SHAP) values (see Section 3.4 for details on SHAP).

studies that investigate how each possible environmental variable drives vertical accretion rates across the wetlands in the MRDP.

Here, we assess the variables that control the time-averaged total vertical accretion (combined organic and inorganic) and its variability in the MRDP. We use a data set of 266 stations from the Coastwide Reference Monitoring System (CRMS) that record vertical accretion and environmental variables. Then, using a machine learning framework, we determine which environmental variables explain accretion rates across the MRDP. Our approach consists of three parts. First, we split our data set by wetland community and use feature selection to determine the variables related to vertical accretion rates. Second, we used the selected features to construct a predictive model for the vertical accretion rates of each wetland community to determine which variables have the most predictive power. Finally, we construct a single unified model for vertical accretion across the delta, where we examine how variables influence accretion within the unified model and explain how this contributes to vertical accretion of wetlands.

2. Data

2.1. CRMS Stations

In this section we summarize the variables collected at each CRMS site that we use in our model. CRMS is a distributed monitoring campaign that is part of an initiative enacted by congress in 1990 in response to the outstanding land loss problem in coastal Louisiana (Couvillion et al., 2017; Steyer, 2010; Steyer et al., 2003). CRMS provides the most comprehensive wetland monitoring database in the world, and it is used for wetland management research and to inform mitigation measures to address the land loss problem (Cortese & Fagherazzi, 2022; Jankowski et al., 2017; Jensen et al., 2022; Keogh et al., 2019, 2021; Sanks et al., 2020). CRMS consists of ~401 stations that record co-located sedimentologic, hydrologic, and biologic data on the wetlands within the MRDP. Each CRMS site also has descriptions of the wetland communities (Figure 1), characterized by the dominant vegetation species as well as the number of present taxa (Visser et al., 2002).

Table 1
Brief Descriptions of the 15 Variables Considered in Our Study, Their Sampling Periods, and Source

Environmental variable	Sampling method	Sampling frequency	Sampling duration	Source
Soil Porewater (ppt)	Insert a water sampling syringe into the upper 10-cm and 30-cm of the soil column	Variable to annually	2007–2022	CRMS
Height Dominant Vegetation (cm)	Height of dominant species determined during surveys by percent of coverage	Annually during peak growing season, July to September	2007–2022	CRMS
Normalized Difference Vegetation Index (NDVI) (unitless)	$\text{NDVI} = \frac{\text{NIR} - \text{Red}}{\text{NIR} + \text{Red}}$ Taken from Landsat 7 imagery	8-day average composite of overlapping images during peak growing season (July to September)	2007–2022	Google Earth Engine
Total Suspended Sediment (TSS, mg/L)	$\text{TSS} = -1.91 * 1{,}140.25$ (SurfaceBand1) Derived from Moderate Resolution Imaging Spectroradiometer Satellite following Miller and McKee (2004)	Recurrence every 2 days	2007–2022	Google Earth Engine
Wind Speed (m/s)	Reanalysis Data from the Global Wind Atlas Database	One characteristic sample	2008–2017	Google Earth Engine
Tidal Amplitude (cm)	Difference between daily high and low water levels	Hourly	2007–2022	CRMS
Average Time Flooded (%)	Percent time the recorded water level exceeds the wetland elevation	Hourly	2007–2022	CRMS
Flood Frequency (Floods/year)	Number of times the recorded water level exceeds the wetland elevation	Hourly	2007–2022	CRMS
Average Flood Depth (cm)	Average recorded water level when the water level exceeds the wetland elevation	Hourly	2007–2022	CRMS
90th Percentile Flood Depth (cm)	90th percentile of the water level when the water level exceeds the wetland elevation	Hourly	2007–2022	CRMS
10th Percentile Flood Depth (cm)	10th percentile of the water level when the water level exceeds the wetland elevation	Hourly	2007–2022	CRMS
Standard Deviation of Flood Depth (cm)	Standard deviation of the water level when the water level exceeds the wetland elevation	Hourly	2007–2022	CRMS
Distance to Water (km)	Distance to nearest 90% recurrence water pixel from the Global Surface Water data set (Pekel et al., 2016)	8-day recurrence	1984–2015	Google Earth Engine
Distance to River (km)	Distance to nearest river vector from the Global River Width from Landsat	1 sample	Satellite era composite	Google Earth Engine
Vertical Accretion Rate (mm/year)	Height of sediment recorded above a feldspar layer datum	6- to 12-month intervals	2007–2022	CRMS

The variable that we are trying to predict is total vertical accretion (combined organic and inorganic sediment) deposited at a CRMS station. Starting in 2007, vertical accretion was measured as the thickness of sediment above a datum, in this case a feldspar layer (Figure 1a, Wager & Haywood, 2022). Vertical accretion measurements are usually retaken every 6–12 months to provide a time series. These temporal measurements are converted into rates by dividing the number of decimal years between establishment and sampling times.

There are many different variables collected at each CRMS station, but we narrowed our focus to 10 hydrologic and sedimentological variables that likely impact sediment transport and deposition processes (Table 1). Hydrologic data, describing tides and flood depths, come from a nearby open water channel on an hourly basis with underwater sondes. The sonde is within 200-m^2 of the monitoring site on dry land. Tidal amplitude is determined from the difference between the highest and lowest water levels within a 24-hr cycle. Flood depths are calculated by subtracting the observed water level from the local land surface elevation of the adjacent monitoring station. The depths we use are the average and 90th percentile values. We use the 90th percentile of flood depth as an indicator of extreme events. It might be expected that the 90th percentile of flood depth co-varies with tides, for

example, during spring tide. While there is a significant relationship (R^2 = 0.065, p-value: 2.5e−5), the 90th percentile of flood depth only explains 6.5% of the variance of tidal amplitude. This suggests that non-tidal flooding processes, perhaps from rivers, hurricanes, or storm surges, may account for the remaining variance.

Sedimentologic data describing soil characteristics, such as grain size, organic matter percentage, organic density, and bulk density, are derived from three 24-cm cores taken upon site initiation and every subsequent 6–10 years. Soil grain sizes are described as percentages of sand, silt, or clay (Wager & Haywood, 2022). Organic matter percentage is measured by dividing the weight of the soil sample after ignition by the dry weight prior to ignition (Wager & Haywood, 2022). Organic density is the mass per volume organic carbon of the soil sample, while bulk density is the density of the sample prior to being dried (Wager & Haywood, 2022).

2.2. Spatial and Remote Sensing Variables From Google Earth Engine (GEE)

We augment the variables from CRMS with five additional variables calculated from Google Earth Engine (GEE): (a) wind speed; (b) distance from a major river; (c) distance to water; (d) normalized difference vegetation index (NDVI); and (e) suspended sediment concentration. Wind speed can be important because it creates waves capable of flooding the wetland platform and delivering resuspended sediment (Allison et al., 2017; Cortese & Fagherazzi, 2022; Mariotti & Carr, 2014). We use wind speed reanalysis data at 250-m resolution collected from the Global Wind Atlas data set, openly available on GEE (*The Global Wind Atlas* 3, 2022). We determined the characteristic wind speed by averaging all values within a 1-km radius surrounding each CRMS station from 2008 to 2017.

Distance from a river is potentially important since river supply of inorganic sediment usually decreases with increasing distance away from the source. We determine the straight-line distance from each CRMS site to the nearest river greater than 30-m wide using the Global River Width from Landsat data set (Allen & Pavelsky, 2018, GRWL). These rivers included the Sabine on the westernmost border, the Pearl on the easternmost border, and the Mississippi and Atchafalaya rivers. Our analysis does not consider whether the river is leveed. Since sediment can come from non-fluvial water sources other than rivers, we calculated the distance of a CRMS station to the nearest water pixel from a 90% water recurrence mask. We use a 90% water recurrence mask to make sure we measure to a persistent water body.

NDVI is commonly used as a proxy for aboveground biomass, which should contribute to vertical accretion provided the organic matter accumulates (Cortese et al., 2023). We acquire NDVI values by computing the 15-year median of 8-day composite Landsat-7 images taken from 1 January 2007 to 1 January 2022. We mask out pixels that occur as water in more than 60% of the images (Pekel et al., 2016), and then computed the average NDVI on all remaining pixels within a 1-km radius of the CRMS stations.

The sediment concentration of water adjacent to the CRMS station may also influence vertical accretion (D. J. Coleman et al., 2022; Cortese & Fagherazzi, 2022; Jensen et al., 2022). Therefore, total suspended solid (TSS) concentrations were estimated from Moderate Resolution Imaging Spectroradiometer Satellite (MODIS) following Miller and McKee (2004). Similar to NDVI, we took all MODIS images within the area represented by CRMS stations from 1 January 2007 to 1 January 2022, this time excluding the land pixels, and calculated the median of all the instances, then averaged the values within a 1-km radius of the CRMS stations. Accretion rates, TSS, wetland communities, the fluvial sources, and the water mask used in our study are shown in Figure 1b.

2.3. Data Preprocessing

The variables from the CRMS sites are collected at multiple times (see sampling frequency in Table 1). To create a characteristic value for each variable that is used in the model, we calculated the median rate over the sampling duration reported in Table 1. For vertical accretion, we do not consider the time history. For all measurements at a given site, we calculated the accretion rate since establishment, and took the median to obtain a characteristic accretion. Following Jensen et al. (2022), stations with accretion rates greater than the 75th percentile plus 1.5 times the interquartile ranges were then removed as outliers, leaving a data set of 266 CRMS stations for analysis (those shown in Figure 1b). A requirement of the machine learning models we apply—a Gaussian process (GP) Regression and a Bayesian Linear Regression (BLR)—is that the data are normally distributed. To ensure this, we transform any variable violating the normality requirement, in this case the distance to water and distance to river variables, by taking the natural log transformation.

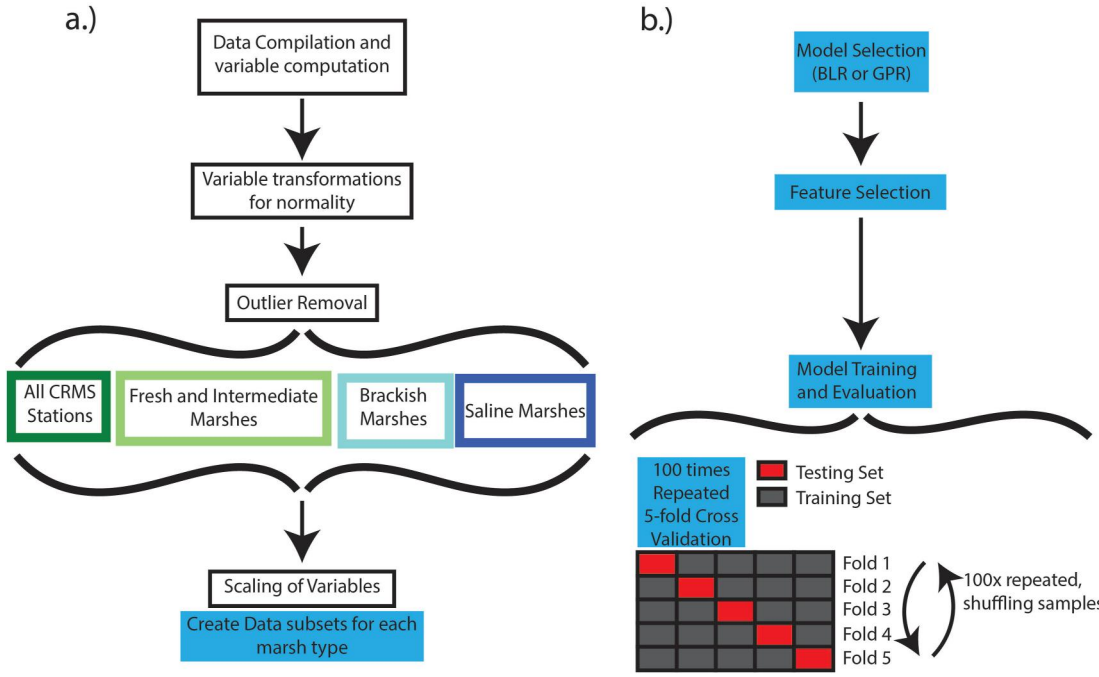

Figure 2. Schematic illustrating the workflow in this study. (a) Preprocessing steps in a machine learning workflow, and (b) Feature selection, implementation, and evaluation of both the Gaussian Process Regression (GPR) and the Bayesian Linear Regression (BLR) machine learning algorithms.

Finally, we scaled our variables before training the machine learning models. This allows the variables to be comparable on equal scales. The scaled equation follows below

$$z_j = \frac{x_j - \overline{x_j}}{S_j} \tag{1}$$

where x_j is the jth input variable, z_j is the scaled x_j, $\overline{x_j}$ is the mean of the jth input variable, and S_j is the standard deviation of the jth input variable.

3. Methods

3.1. Machine Learning Workflow

In this section, we refer to the 15 input variables listed in Table 1 as *variables* and the resulting calculation of time-averaged vertical accretion as the *target* prediction. Our goal is to identify the most important variables contributing to accretion rates. During our initial exploration and consistent with published studies (e.g., Brown et al., 2017), we found that different marsh communities may influence modes of accretion (Figure 1). Because of this, we split our data into three experimental sets. These sets are determined by the reported marsh type at the CRMS station: (a) freshwater-intermediate marshes, (b) brackish marshes, and (c) saline marshes. We split the data into marsh community groups since variables that influence accretion, such as salinity, tidal amplitude, and NDVI, vary across marsh communities (Jarvis, 2010; Lane et al., 2020). We first preprocess the data as shown in Figure 2a, then, for each of the three experimental sets, we conduct feature selection to determine which variables in Table 1 influence accretion rate and should be used in the model (Figure 2b). CRMS stations in swamp communities were excluded from this study because there are no recordings of sedimentologic characteristics for the sites.

Due to the number of CRMS stations per marsh community subset, we used backward elimination for feature selection (Han & Kamber, 2012). It involves fitting an ordinary least squares regression with the variables in Table 1 as independent variables and the accretion rate as the dependent variable for each experimental set. The p-value is computed for each independent variable, removing the variable with the highest p-value and repeating the

process until all variables have a p-value below the significance threshold of 0.05. This final set of significant variables is used in the final model. We evaluate the performance of our final model by randomly splitting the data into 5 equally sized subsamples, training our model on four of the subsamples, testing our trained model on the remaining subsample (called 5-fold cross validation), and repeating that 100 times (Figure 2b). Below we explain the machine learning algorithms, a Gaussian Process Regression (GPR) and a BLR, which we implement using the Python machine learning package *scikit-learn*.

3.2. Bayesian Linear Regression (BLR)

We use a BLR for two reasons. First, because feature selection is judged by ordinary least squares, implementing a linear model, like the BLR, is a logical way forward. Second, BLR is an interpretable model (Bishop, 2006; Molnar, 2019) because it approximates the unknown target $f(x)$ from a linear combination of the input variables, x (Table 1). BLR is also has a regularization term, which limits data overfitting. The Bayesian treatment of linear regression allows us to solve for the regularization term without hyperparameter tuning, which would require splitting our data set into smaller subsets. When we insert our regularization term, our solution to the weight vector then follows

$$w_{\mathrm{ML}} = \left(\frac{\alpha}{\beta} I + X^T X\right)^{-1} X^T y \tag{2}$$

where y is the target variable, β is the noise associated with y, α is the noise associated with the weight parameter w, I is the identity matrix, and X is the set of input variables. The value of $\frac{\alpha}{\beta}$ is the regularization term.

The BLR model works best when the input variables are all scaled within the same range of values because the learned weight coefficients are proportional to feature importance. However, when we interpret how the variables affect the target in their natural units, we transform them back to their original units. When transformed, we can interpret the coefficients in the classic sense that an increase in x_j, the jth variable, will increase y according to the magnitude of the weight coefficient for the jth variable. Thus, we report feature importance derived from the mean absolute value of the scaled weight coefficients and use the mean of the transformed weight coefficients for interpretation.

3.3. Gaussian Process Regression (GPR)

At the whole delta scale, we opt for a nonlinear model that can handle the differing controls on accretion per marsh community. The nonlinear model that we use is a GPR, which is a probabilistic machine learning technique that can make predictions about a target for any input variable. The GPR model overcomes linearity by projecting the input variables into an infinitely high dimensional space using basis functions (Rasmussen & Williams, 2005).

A GPR models the target as a GP, which is a collection of random variables that follow a multivariate Gaussian distribution. The GP can be completely specified by its mean function, $m(x)$, and covariance function, $k(x,x')$ (Rasmussen & Williams, 2005). With a known mean and covariance, the prior distribution of all possible random unknown functions is

$$f(x) \sim \mathrm{GP}\left(m(x), k\left(x,x'\right)\right) \tag{3}$$

An important choice for GPR is the covariance function, $k(x, x')$, which represents the uncertainty in the data. In a broad sense, we expect similar samples to have similar outcomes and effects on the target variable and their covariance function is what defines the similarity between samples. After multiple trials, we deduce that a squared dot product covariance function fits our use case

$$k\left(x,x'\right) = \left(x \cdot x'\right)^2 + \delta \tag{4}$$

where δ is the error associated with the target variable, the vertical accretion rate, and x and x' are either variables within the training or test sets, as seen in Equation 5.

From a specified mean and covariance function, the joint distribution of our observed target values and the functions of every given test sample is given as

$$\begin{matrix} y \\ f_* \end{matrix} \sim \mathcal{N}\left(\begin{matrix} 0 \\ 0 \end{matrix}, \begin{matrix} k(X,X)+\sigma^2 I & k(X,X_*) \\ k(X_*,X) & k(X_*,X_*) \end{matrix}\right) \tag{5}$$

where $k(X, X)$ is the variance within training samples, $k(X_*, X_*)$ is the variance within testing samples, $k(X_*, X)$ and $k(X, X_*)$ are the covariances between training and testing samples, y is the target variable, f_* is the learned predictive function, and σ^2 is the noise associated with the target variable (Rasmussen & Williams, 2005). Equation 5 assumes a zero mean. Utilizing the rules for the combination of partitioned Gaussians, the mean and covariance for the predictive posterior distribution for f_* are

$$m(x) = k(X_*,X)\left(k(X,X)+\sigma^2 I\right)^{-1} y \tag{6}$$

$$k(x,x') = k(X_*,X_*) - k(X_*,X)\left(k(X,X)+\sigma^2 I\right)^{-1} k(X,X_*) \tag{7}$$

3.4. Post-Training Explainability: SHAP

To attain transparency of predictions from the GPR model, we make use of a readily available python package for post training explainability called SHapley Additive exPlanations (SHAP). SHAP computes the Shapley values for individual predictions for various machine learning models (Lundberg & Lee, 2017). Acquired from game theory, Shapley values seek to quantify the relative involvement of players in a game. In our case, the "players" are the variables from Table 1 included in the GPR model, and the "game" is the task of predicting vertical accretion rates.

To evaluate the contribution of each variable, the explainability model can be regarded simply as

$$\hat{f}(x) = \bar{f}(x) + \sum_{j=1}^{M} \phi_j \tag{8}$$

where $\hat{f}(x)$ is the predicted target, $\bar{f}(x)$ is the mean of all the predicted values, and ϕ_j is the Shapley value contribution of the jth variable of M total variables (Silva et al., 2022).

Individual Shapley values come from the relative influence of each variable on a single sample of the predictions. This is done by calculating the differences between the predictions, including and excluding the variable of interest for every possible combination of variables for a total of 2^M combinations of variables. For example, if we are interested in the Shapley value of jth variable, using our GPR model we compute the estimated outcome including the jth variable for each sample, compute the estimated outcome excluding the jth variable for each sample, and then subtract the two estimations from each other. The difference is the Shapley value, and the average difference across all 2^M values expresses how much the jth variable influences a prediction.

4. Results

4.1. Bayesian Linear Regression (BLR) Experiments

The BLR models for each marsh community reveal two important findings. First, certain marsh subsets have higher predictive capabilities than others (Figure 3). The freshwater-intermediate ($n = 150$) and saline marsh ($n = 57$) subsets yield the highest R^2 values of 42% and 50% respectively. The brackish marsh ($n = 59$) subset, situated between fluvial and oceanic sources, has the lowest R^2 value of 20%.

Second, each marsh type has a unique set of significant environmental variables that influence sedimentation (Figure 4). Because the model was trained on scaled variables (Equation 1), the magnitudes of the weights from a single model can be directly compared to assess relative feature importance (Molnar, 2019). Larger values are features of higher importance than those with lower values. However, feature importance values are model specific and cannot be compared across models, which is why we use the term "relative" feature importance. For

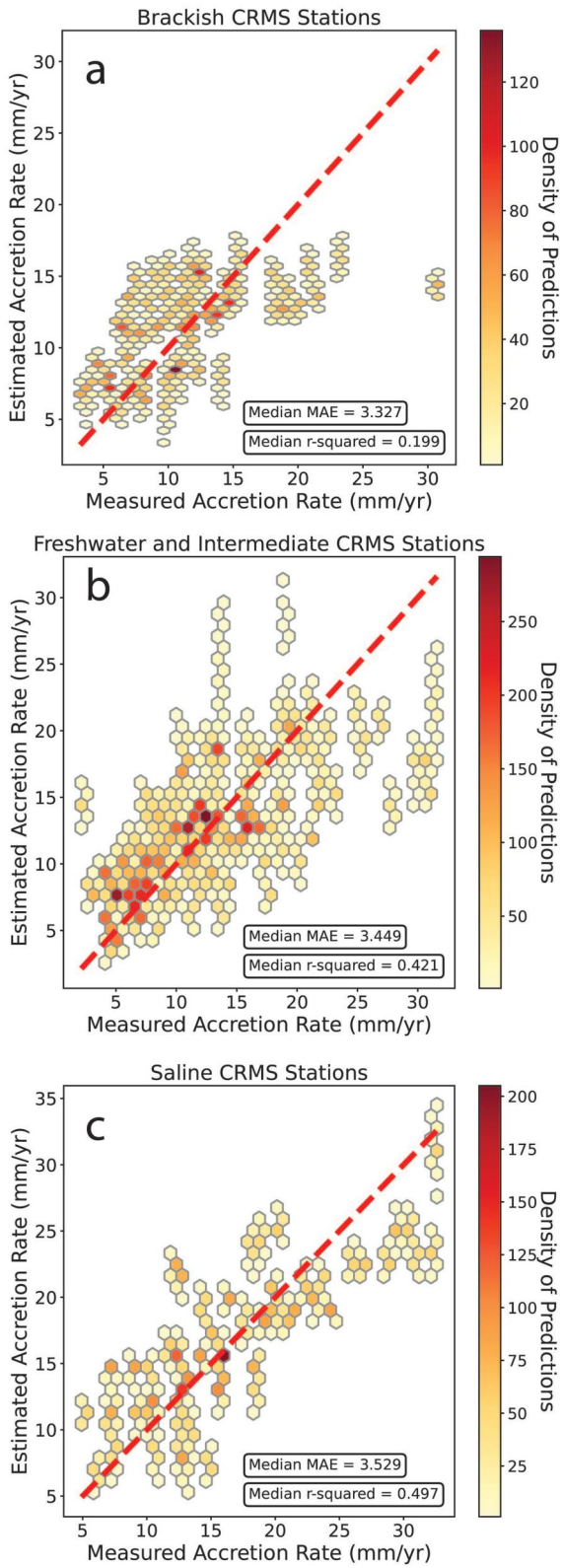

Figure 3. Cross validation predicted vertical accretion rates versus measured vertical accretion rates for each wetland type (a–c). Honeycomb cells represent the density of predictions versus observed values.

freshwater and intermediate marshes, tidal amplitude was the most important, while soil porewater salinity, total suspended sediment, wind speed, flood frequency, distance to water, and the 90th and tenth percentile flood of flood depths played secondary roles (Figure 4b). In the brackish marsh subset, the number of important variables decreases and only includes soil porewater salinity and the average height of the dominant vegetation type (Figure 4a). Lastly, in the saline marshes, NDVI, total suspended sediment, the 90th percentile of flood depth, and the tenth percentile of flood depth are important (Figure 4c). Not surprisingly, vertical accretion in all of the marsh types depends more on hydrodynamic variables, such as flooding, except in the brackish marshes, where vegetation parameters emerge as more important.

Transforming the weight coefficients into their natural units reveals the positive or negative influence of each variable on the model. Consistent with expectations, TSS and flood-related variables (e.g., tidal amplitudes, flood depth percentiles, and flood frequencies) were always positive contributors to vertical accretion predictions. Negative contributions to vertical accretion rates were from soil porewater salinity, NDVI, and windspeed of the experimental sets.

4.2. Gaussian Process Regression (GPR) Experiments

There is not a straightforward way to conduct feature selection for nonlinear dependencies, so we choose which variables to use in our GPR model by selecting the most important variables from the BLR models for each marsh community subset. These are tidal amplitude and TSS for the freshwater-intermediate subset, soil porewater salinity for the brackish subset, and NDVI and the 90th percentile of flood depth for the saline subset. Considering all these variables in a GPR model captures the differing controls on sedimentation across marsh types.

Using the 5-fold cross-validation technique to determine our model fit (splitting the data set into 5 equal subsets, training and testing, then repeating 100 times), we achieve an $R^2 = 0.47$ (Figure 5). Because GPR models the interactions between variables, the results cannot be interpreted as directly as the BLR because variables are not independent. To circumvent this, we computed the feature importance from Shapley values (Figure 6a), waterfall plots (Figure 6b), and dependence plots of features (Figures 7a, 7d, 8a, 8d, and 9a). The notation $(*)$ denotes that the variable is in the scaled units of standard deviations.

The mean SHAP value reveals the relative importance of each variable in the GPR model (Figure 6a). This is calculated by averaging the SHAP values associated with a single variable such as tidal amplitude (e.g., Figure 6b) across all CRMS predictions and taking the absolute value. The most important variable is tidal amplitude, followed by NDVI, soil porewater salinity, 90th percentile flood depth, and total suspended solids (Figure 6a).

The prediction of vertical accretion for each CRMS is created through a combination of different variables, which can be visualized in a waterfall plot (Figure 6b). Looking at CRMS0171, located in the Barataria basin (Figure 1), the ribbons show the SHAP value of each variable and its effect on the final prediction of accretion $f(x)$, where tidal amplitude causes the largest increase in accretion (relative to the mean of all predictions, $E[f(x)]$) and soil porewater salinity causes the largest decrease (Figure 6b). The SHAP values show how each variable causes the model prediction to deviate from the mean

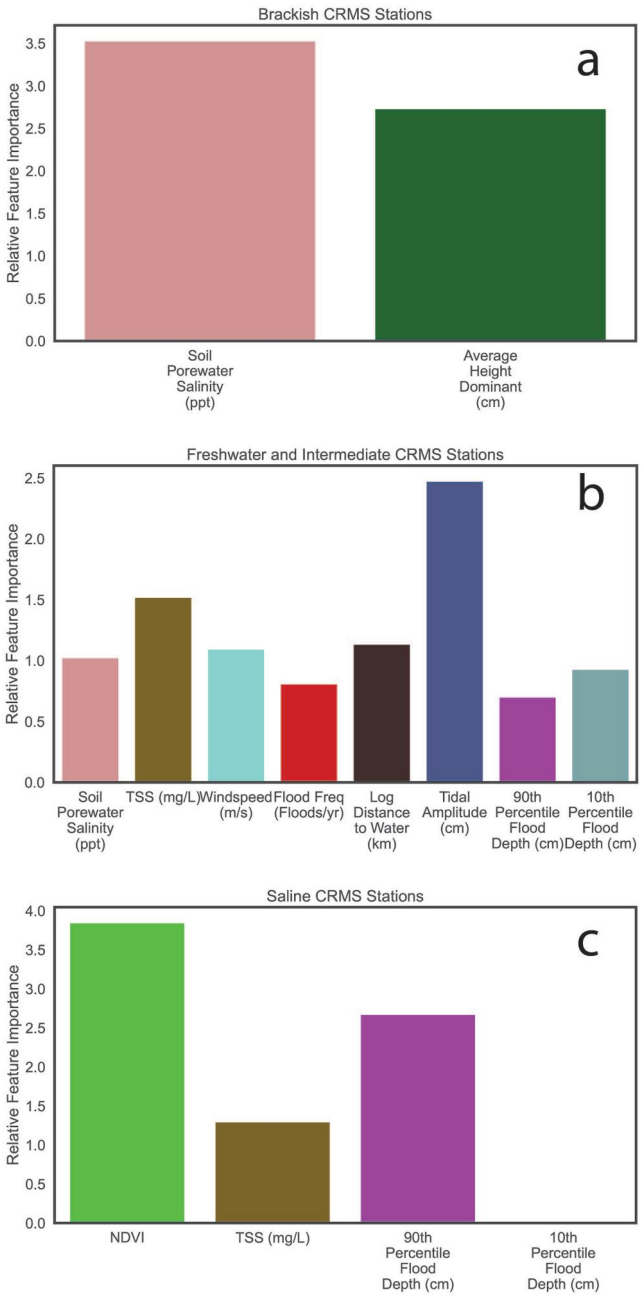

Figure 4. The relative importance of each feature within the Bayesian Linear Regression models for each wetland type (a–c) determined from the absolute value of the average of the 500 learned weight coefficients for each experimental set.

prediction for all stations ($E[f(x)]$). Thus, the SHAP values are dimensional and sum to a single prediction $f(x)$, which in Figure 6b is 17 mm/year.

To understand how tidal amplitude, for instance, affects all predictions rather than the single one in Figure 6b, we can use SHAP dependence plots. The SHAP dependence plots show the SHAP value (i.e., the ribbon in Figure 6b) of a single variable for every CRMS station prediction and express the relative influence of a variable on vertical accretion across all samples. These are colored by the magnitude of another related variable in the model to help visualize interactions between variables.

Tidal amplitude is identified as the most important variable in the GPR model (Figures 7a–7c). Up to a tidal amplitude of 1.0*, larger amplitude tides enhance sedimentation, but at amplitudes >1.0* the relationship becomes less clear (Figures 7a and 7c). The spreading corresponds to changes in the 90th percentile flood depth where high tides are correlated with high sedimentation when flood depths are large (Figure 7a). Large tidal amplitudes tend to occur more commonly in saline marshes (Figure 7b).

The 90th percentile flood depth is important for sediment transport and its subsequent deposition. Higher flood depths have higher contributions to accretion (Figures 7d and 7f). Though the effect depends on tidal amplitude, as sites with low tidal amplitudes seem to be less responsive to increasing 90th percentile flood depths, while sites with high tidal amplitudes have a stronger response to increasing flood depths (Figure 7d). There does not seem to be any clear separation of the distributions of flood depths per marsh community (Figure 7e).

NDVI is the second most important variable, and it has a nonlinear and non-monotonic influence on accretion (Figures 8a–8c). Moving from low to the mean value (0*), the contribution of NDVI to accretion is positive but diminishes and eventually becomes negative (meaning it decreases accretion relative to the mean). As NDVI increases above the mean value, its contribution to accretion is negative but grows and eventually becomes positive again (Figure 8a). These differences correlate with salinity values: when porewater salinity levels are high, there is a diminishing relationship between NDVI and accretion, but when porewater salinity is low, the relationship reverses (Figures 8a and 8c). This is related to different marsh types. The mean unscaled value of NDVI is roughly 0.35, which also marks a clear split in the marsh type (Figure 8b). This suggests that the effect of NDVI on accretion in our model is different for freshwater-intermediate marshes and saline marshes.

Soil porewater salinity displays a negative linear relationship with vertical accretion (Figures 8d–8f). NDVI levels are highest where salinity is lowest, verifying a dependence of salinity and NDVI (Figures 8a, 8d, and 8f). As expected, the distribution of salinity values shows that there is a separation between freshwater-intermediate and brackish-saline sites around 10 ppt (Figure 8e).

Finally, higher TSS concentrations lead to higher vertical accretion rates (Figure 9a). TSS is largely independent of the other variables considered in the model, as indicated by the minimal interactions in the SHAP dependence plot (Figure 9a). But higher TSS is associated with slightly higher bulk densities (Figure 9c). There is also little separation in the distribution of TSS across marsh types (Figure 9b). Therefore, it seems to act solely as a positive contributor to vertical accretion for all marsh communities, contrasting the role of soil porewater salinity (Figures 8d and 9a).

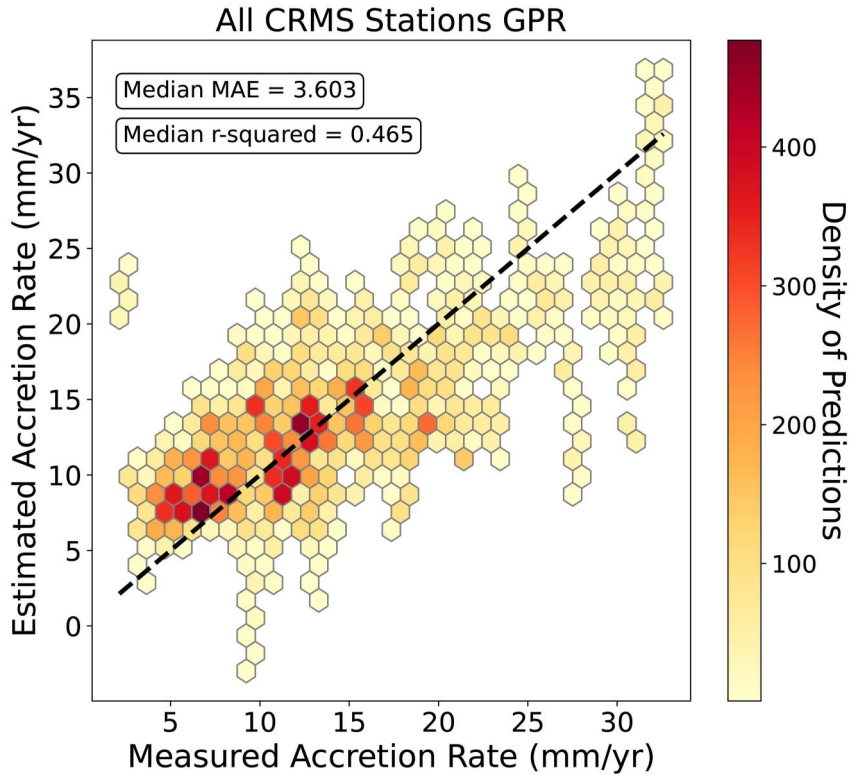

Figure 5. Predicted vertical accretion rate versus observed vertical accretion rate for the 500 splits of the cross-validation simulations (5-fold cross-validation repeated 100 times) in the Gaussian Process Regression (GPR) experiment.

5. Discussion

5.1. The Influence of Tidal Amplitude, 90th Percentile Flood Depth, and NDVI

Our discussion revolves around our GPR model because it integrates the whole delta while performing reasonably well on prediction tasks. The GPR model shows that the vertical accretion rate of sediment is controlled by tidal amplitude, NDVI, and porewater salinity, whereas flood depth, and TSS are of secondary importance (Figure 6a). While this is not necessarily novel, it is consistent with a large body of field work (Baustian et al., 2020; Bianchette et al., 2015; Brown et al., 2017; Callaway et al., 1996; Lane et al., 2020; Nyman et al., 2006). But, in field deployments, it can be difficult to isolate variables and extrapolate findings over a broader area. Our methodology and results shed light on how these variables work together. For example, the tidal range is the most important variable in our model because tidal flooding of the wetland surface transports inorganic sediment into the system. Other variables related to flooding, such as 90th percentile flood depth, achieve a similar outcome but are not as important. The model indicates that these two variables are additive because sites with large flood depths and large tidal ranges have the highest accretion rates (Figures 7a and 7d). Highlighted in Figure 1 in yellow are sites that have both flooding depths and tidal amplitudes greater than the 75th percentile of their respective distributions. The reasons why flooding enhances vertical accretion more effectively at high amplitudes are possibly because of the position of the marshes. Among these 14 CRMS stations with high tidal amplitudes and high flooding depths, three of them are located close to an active fluvial sediment source such as the Mississippi River delta. The other 11 are in the Terrebonne and Barataria basins where some of the highest land loss rates are measured (Couvillion et al., 2017). In Terrebonne and Barataria, edge erosion could be a significant source of sediment for vertical accretion (Cortese & Fagherazzi, 2022; Edmonds et al., 2023; Sanks et al., 2020). It seems that sites with high tides and deep flooding could have higher vertical accretion because of additional sediment sources.

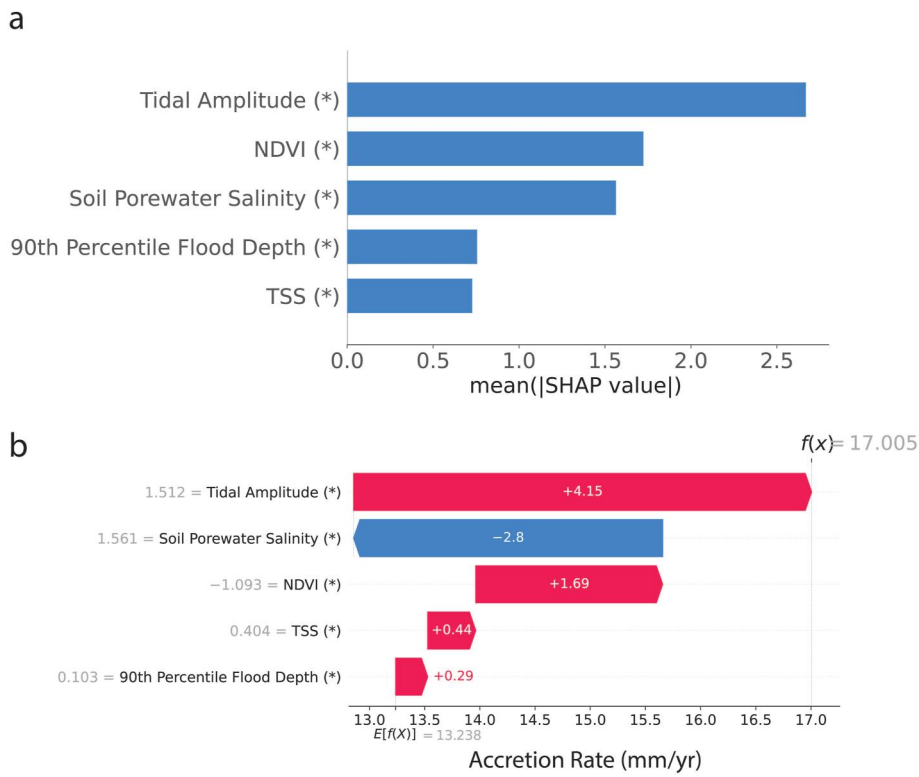

Figure 6. (a) Feature importance of variables within the Gaussian Process Regression (GPR) model as defined by mean SHapley Additive exPlanations (SHAP) values. The size of the bar, arranged from most important to least important, indicates the relative importance of the variable to the GPR model. These values are created by averaging all the SHAP values for each variable across all stations and taking the absolute value. (b) Waterfall plot showing the unscaled SHAP values for different variables at CRMS0171 that influence the final prediction of accretion within our model. $E[f(x)]$ is the mean of all vertical accretion predictions across all Coastwide Reference Monitoring System stations, and 17.005 mm/year is the vertical accretion prediction for CRMS0171.

NDVI is the second most important variable for predicting accretion in our GPR model (Figure 6a) and it may be important because it represents aboveground biomass, which is a sediment source. This assumption was made by Jensen et al. (2022), who chose to use it in a predictive model for vertical accretion. To test the validity of this assumption, we used aboveground biomass estimates for 146 CRMS stations from the Coastal Information Management System website. We found no clear relationship between NDVI and aboveground biomass or organic matter in the soil (Figure 10). This contradicts the results of Cortese et al. (2023), and this might arise because our study covers the whole MRDP, which could introduce more variability. The lack of relationship could be because a significant portion of organic matter deposited on the marsh surface is allochthonous material transported during floods rather than through in situ production and subsequent deposition (Mariotti et al., 2020).

Flood depth seems to negatively bias the NDVI values in our data set (Figure 11). This is not altogether surprising because water has lower NDVI values (Kearney et al., 2009; Mo et al., 2017; Narron et al., 2022; Suir & Sasser, 2019; Sun et al., 2018). However, there are two negative trends with different slopes: a shallow trend that includes mostly freshwater-intermediate marshes and a steep trend that traverses all marsh communities (Figure 11a). The steeper sloped trend traverses a salinity gradient described by the changing marsh communities (Figures 11a and 11c), which likely amplifies the negative relationship between NDVI and flood depth. These two trends are not caused by inundation effects because the shallow trend has the highest inundation times (Figure 11b). Nevertheless, inundation does seem to reduce NDVI because within each trend, sites with lower NDVI also have higher inundation. But a more likely reason for the separation of the two trends is that the unique vegetation species of each marsh community are recorded by NDVI, either by differences in plant litter background color or other characteristics.

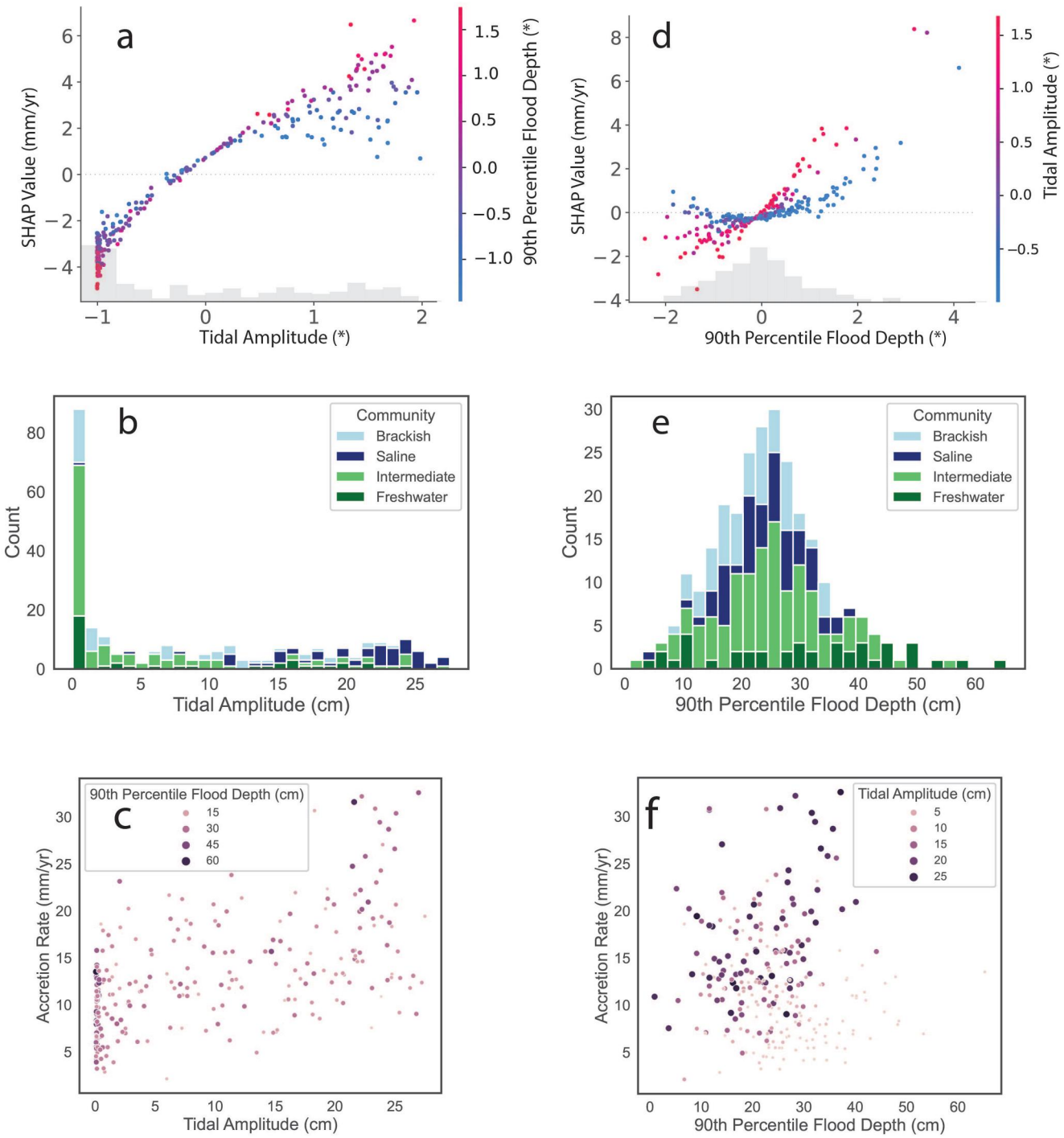

Figure 7. (a, d) SHapley Additive exPlanations (SHAP) dependence plot for tidal amplitude and flood depth. The *x*-axis is the scaled variable and the *y*-axis is the SHAP value. The points correspond to different Coastwide Reference Monitoring System stations and are colored by the scaled values of a given variable. The gray bars directly above the *x*-axis show the distribution of the scaled *x*-axis variable. (b, e) Distribution of the variable for each marsh community type. (c, f) Unscaled Scatter plots between variables of interest.

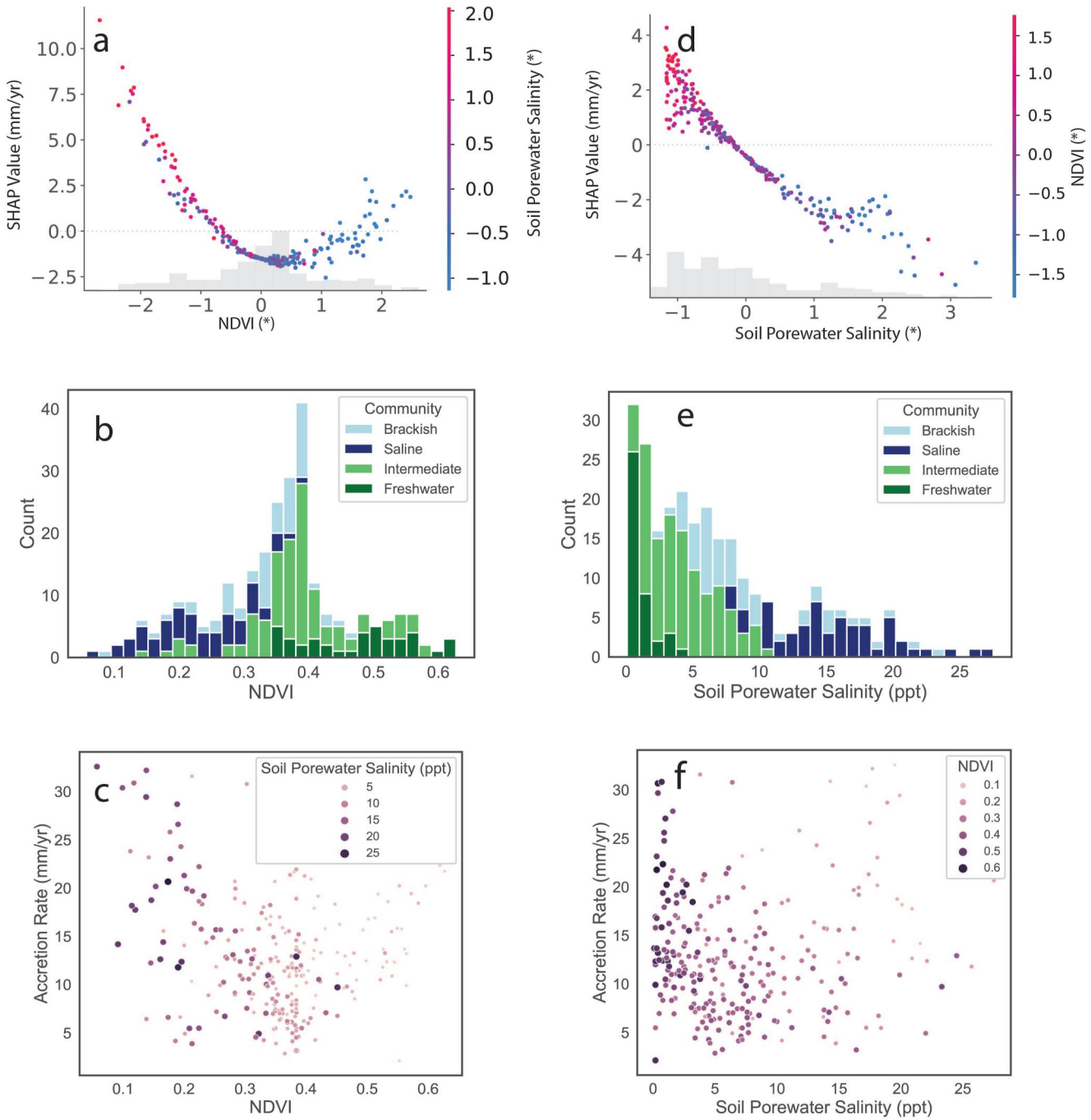

Figure 8. (a, d) SHapley Additive exPlanations (SHAP) dependence plot for normalized difference vegetation index (NDVI) and soil porewater salinity. The *x*-axis is the scaled variable and the *y*-axis is the SHAP value. The points correspond to different Coastwide Reference Monitoring System stations and are colored by the scaled values of a given variable. The gray bars directly above the *x*-axis show the distribution of the scaled *x*-axis variable. (b, e) Distribution of the variable for each marsh community type. (c, f) Unscaled Scatter plots between variables of interest.

It is clear that NDVI records more than aboveground biomass because it is also affected by flooding regimes and varying plant compositions (Cortese et al., 2023). It seems that the main function of NDVI in the GPR model is to distinguish marsh communities, which is consistent with the findings of Cortese et al. (2023) for the Terrebonne Basin. Our data suggest that NDVI is an important feature in the models because it distinguishes marsh communities that depend on different sources of sedimentation.

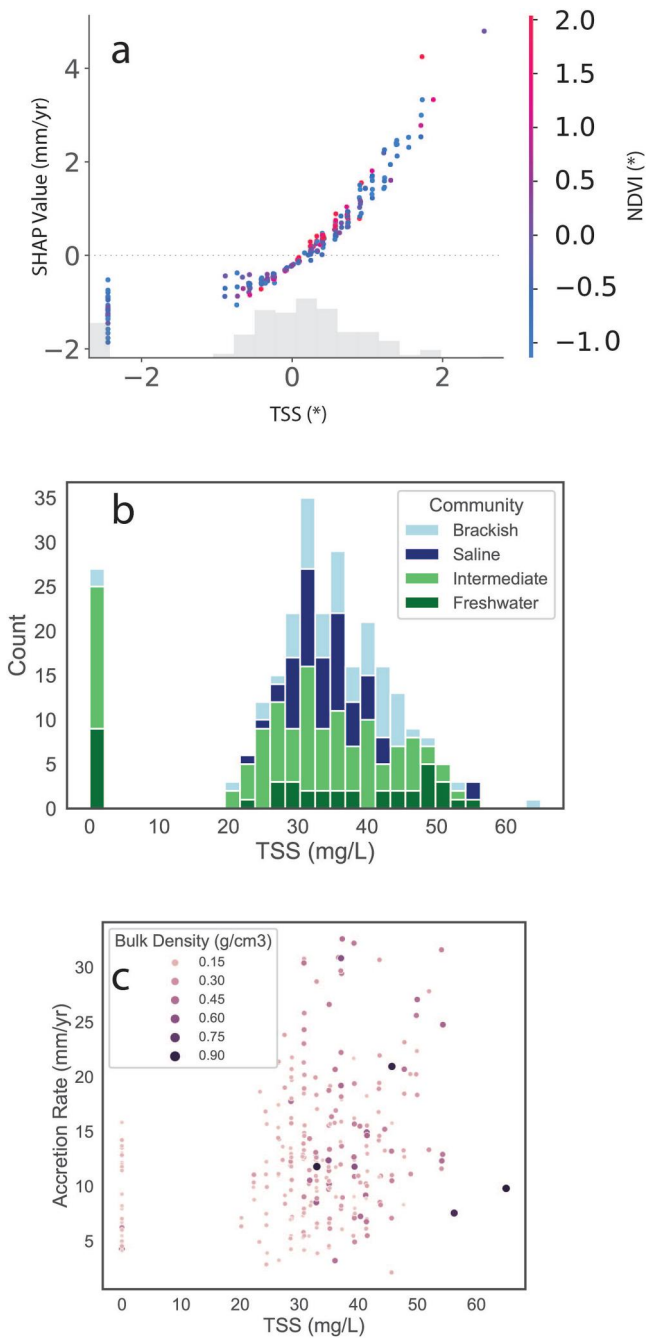

Figure 9. (a) SHapley Additive exPlanations (SHAP) dependence plot for total suspended solids (TSS). The *x*-axis is the scaled variable and the *y*-axis is the SHAP value. The points correspond to different Coastwide Reference Monitoring System stations and are colored by the scaled values of a given variable. The gray bars directly above the *x*-axis show the distribution of the scaled *x*-axis variable. (b) Distribution of the variable for each marsh community type. (c) Unscaled Scatter plots between variables of interest. Scatter plot markers are colored by bulk density (a term not included in the ML framework).

5.2. Variability of Vertical Accretion Rates

Our study has contributed predictions of accretion rates across the coast of Louisiana using a small set of five environmental variables with a GPR model. Our model R^2 values suggest that half of the observed variation in accretion is explained by the model (Figures 3 and 5). Our model's R^2 is similar to that reported for the Integrated Compartment Model used in the 2017 and 2023 Coastal Master Plan (Brown et al., 2017). That model, however, is based on the mass balance of water and sediment, and is driven by field-derived boundary conditions. The fact that these two vastly different approaches yielded similar results underscores just how noisy accretion rates are and how difficult they are to predict. Part of the issue could be that the CRMS accretion data have short spatial correlations of the order of 10 km (Nienhuis et al., 2017; Sanks et al., 2020). The relatively low R^2 values of the model here could be an outcome of using gradually varying properties (like tidal range or NDVI) to predict noisy accretion measurements that vary considerably from site to site.

It seems that higher resolution measurements in space or time could improve predictions with these variables. An obvious place to start is with the sediment supply side of vertical accretion. The TSS values we derived from MODIS, arguably a dominant source of inorganic sediment, gradually vary and are averaged over 15 years. If vertical accretion is primarily event-driven, then future approaches might try predicting the time-dependent accretion rate at a given site with variables such as TSS calculated over the same sampling period.

In particular, our model underperforms at the highest accretion rates. This could be because these sites with high vertical accretion have sediment sources not reflected in our variable list. One possibility is the local recycling of sediment from edge erosion of the wetland. Sanks et al. (2020) speculated this could be a source of sediment, and Edmonds et al. (2023) suggested that edge erosion may account for up to 80% of the mineral sediment in the Barataria Basin. Another possibility is that storms are the cause of the high vertical accretion. Water level increases from storms should be recorded in the 90th percentile flooding depth, but isolating that effect is not straightforward. Previous studies have noted that storms rework sediment along the coast, causing substantial elevation changes (Bianchette et al., 2015; Cahoon et al., 2006; Cortese & Fagherazzi, 2022; Hopkinson et al., 2018; Howes et al., 2010; Thorne et al., 2022; Turner et al., 2006). Thus, discerning the main drivers of accretion during extreme storm events can be an exciting avenue of future research.

Another possibility for the lower performance of the model at high accretion rates is shallow subsidence. We specifically measure vertical accretion, which depending on the local shallow subsidence (Jankowski et al., 2017) may or may not result in positive surface elevation change. If sites with high vertical accretion also induce higher shallow subsidence and decrease in surface elevation, then that positive feedback creates accommodation space that could continue to encourage vertical accretion. It is not clear how this effect might be picked up in the variables used in our models.

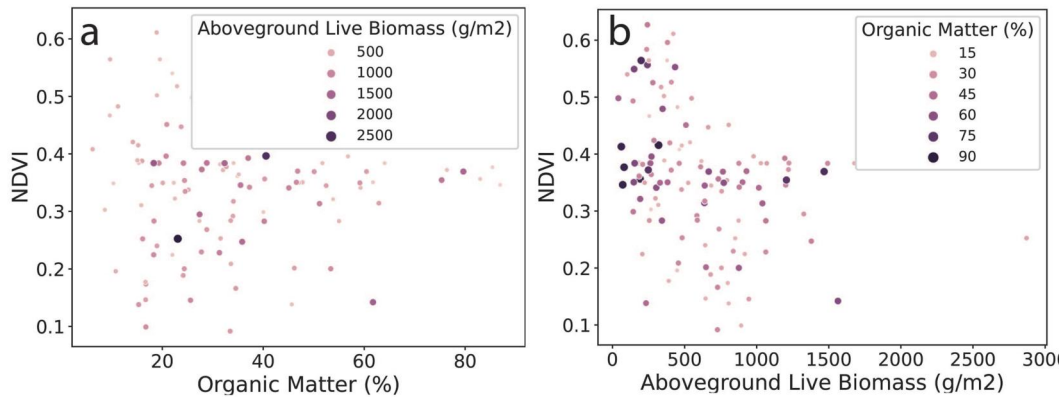

Figure 10. Using a data set of 146 Coastwide Reference Monitoring System (CRMS) stations, (a) There is no correlation between normalized difference vegetation index (NDVI) and percent organic matter within the top 24-cm of soil at a CRMS station. (b) There is little correlation between NDVI and aboveground biomass.

6. Conclusion

The sustainable management of the MRDP relies on understanding the sedimentation rate and patterns. But in a complex wetland system, where biologic, chemical, and physical processes interplay, the drivers of sedimentation are multifaceted. The CRMS on the MRDP maintains 266 sites where vertical accretion is regularly measured.

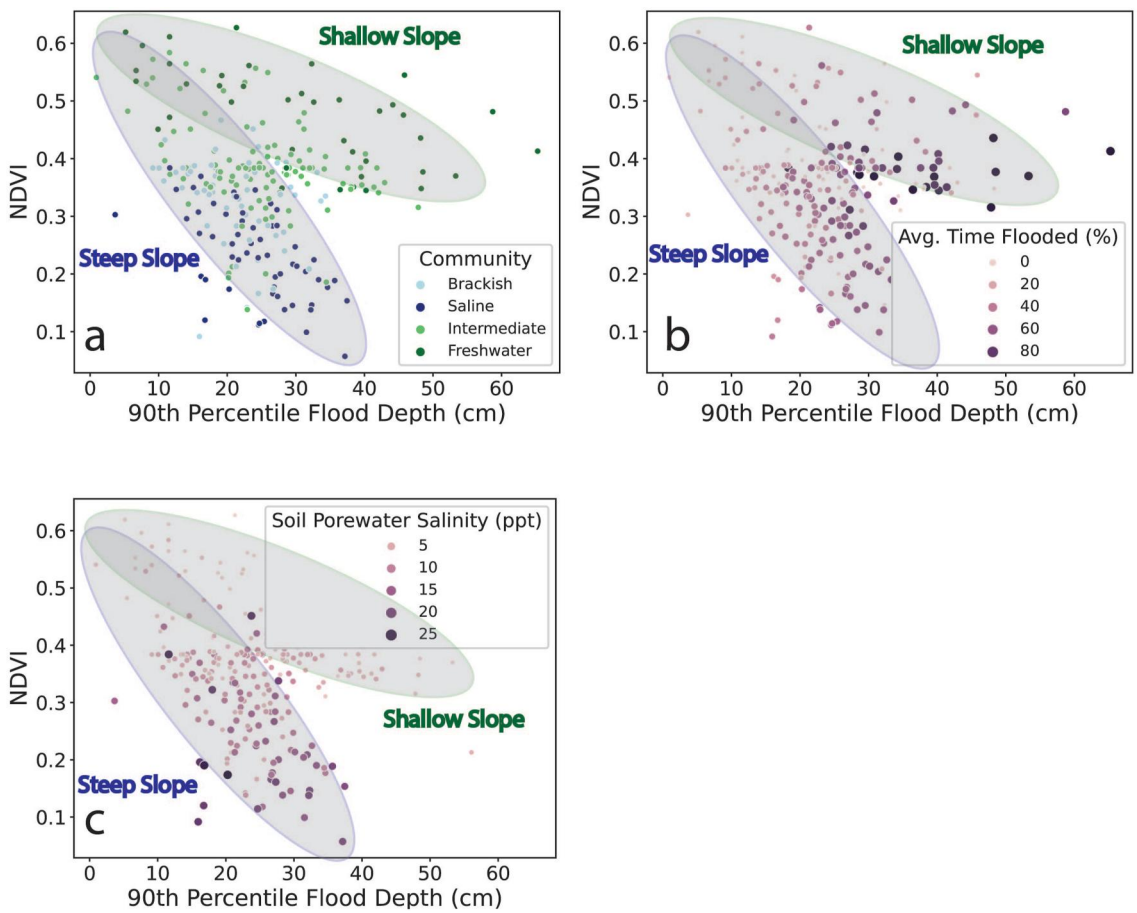

Figure 11. Plots of normalized difference vegetation index (NDVI) and 90th percentile flooding depth for all points used in the Gaussian Process Regression model. Panels (a, b, and c) differ only in how the points are colored or displayed.

We use this data and a machine learning framework to understand the sedimentology, hydrodynamic, and ecological controls on vertical accretion. Even in a microtidal system, our model clearly identifies the importance of tidal amplitude on vertical accretion. High tidal amplitude increases sedimentation even more when it co-occurs with a large flooding depth. NDVI has a nonlinear influence, primarily recording shifting flooding and plant community gradients rather than aboveground biomass. We corroborate previous notions about the tendency of saline intrusions to act as sinks of sediment volume and suspended sediment in nearby waters to act as a source of sediment volume. While our predictive models have an R^2 ranging from 20% to 50%, we find that highly accurate accretion predictions in the mixed marshes of Louisiana remain difficult. Two prominent avenues of future work may help improve the predictions. First, a focused study aimed to achieve a clear explanation for how tidal amplitude can capture much of the variability of accretion in Louisiana would clarify its importance in depositional processes. Second, exploring the NDVI gradient across coastal Louisiana and its effects on vertical accretion rates would prove insightful as more marshes transcend from brackish to saline marsh types as relative sea levels continue to rise. Incorporating this knowledge into future models of deltaic deposition could inform coastal practices and management in a changing natural and human landscape.

Data Availability Statement

Code and relevant data files can be found on Zenodo (Chenevert, 2023). All data were derived from the Coastal Reference Monitoring System and Costal Information Management System (Coastal Protection and Restoration Authority, 2023).

Acknowledgments
DAE and EC acknowledge funding from Indiana University and funds from the Malcolm and Sylvia Boyce Chair. J. Gearon, H. Martin, and J. Han are thanked for discussions about this work. We thank J. Shaw, X. Liu, R, Steele, and one anonymous reviewer for comments that improved this paper.

References

Allen, G. H., & Pavelsky, T. M. (2018). Global extent of rivers and streams. *Science*, *361*(6402), 585–588. https://doi.org/10.1126/science.aat0636

Allison, M., Chen, Q. J., Couvillion, B., Freeman, A., Leadon, M., McCorquodale, A., et al. (2017). *2017 Coastal master plan: Model improvement plan, attachment C3-2: Marsh edge erosion*. Version Final (pp. 1–51). Coastal Protection and Restoration Authority.

Barbier, E. B., Georgiou, I. Y., Enchelmeyer, B., & Reed, D. J. (2013). "The value of wetlands in protecting southeast Louisiana from hurricane storm surges." Edited by Gil Bohrer. *PLoS One*, *8*(3), e58715. https://doi.org/10.1371/journal.pone.0058715

Baustian, M. M., Reed, D., Visser, J., Duke-Sylvester, S., Snedden, G., Wang, H., et al. (2020). *2023 Coastal master plan: Attachment D2: ICM-Wetlands, vegetation, and soil model improvements*. Version 2 (p. 90). Coastal Protection and Restoration Authority.

Baustian, M. M., Stagg, C. L., Perry, C. L., Moss, L. C., & Carruthers, T. J. B. (2021). Long-term carbon sinks in marsh soils of coastal Louisiana are at risk to wetland loss. *Journal of Geophysical Research: Biogeosciences*, *126*(3), e2020JG005832. https://doi.org/10.1029/2020JG005832

Baustian, M. M., Stagg, C. L., Perry, C. L., Moss, L. C., Carruthers, T. J. B., & Mead, A. (2017). Relationships between salinity and short-term soil carbon accumulation rates from marsh types across a landscape in the Mississippi River Delta. *Wetlands*, *37*(2), 313–324. https://doi.org/10.1007/s13157-016-0871-3

Bianchette, T., Liu, K.-B., Yi, Q., & Lam, N. (2015). Wetland accretion rates along coastal Louisiana: Spatial and temporal variability in light of hurricane Isaac's impacts. *Water*, *8*(1), 1. https://doi.org/10.3390/w8010001

Bishop, C. M. (2006). *Pattern recognition and machine learning*. In *Information science and statistics*. Springer.

Blum, M., Rahn, D., Frederick, B., & Polanco, S. (2023). Land loss in the Mississippi River Delta: Role of subsidence, global sea-level rise, and coupled atmospheric and oceanographic processes. *Global and Planetary Change*, *222*, 104048. https://doi.org/10.1016/j.gloplacha.2023.104048

Blum, M. D., & Roberts, H. H. (2009). Drowning of the Mississippi Delta due to insufficient sediment supply and global sea-level rise. *Nature Geoscience*, *2*(7), 488–491. https://doi.org/10.1038/ngeo553

Blum, M. D., & Roberts, H. H. (2012). The Mississippi Delta Region: Past, present, and future. *Annual Review of Earth and Planetary Sciences*, *40*(1), 655–683. https://doi.org/10.1146/annurev-earth-042711-105248

Brown, S., Couvillion, B., Conzelmann, C., de Mutsert, K., Fischbach, J., Hunnicutt, C., et al. (2017). *2017 Coastal master plan: Appendix C: Modeling Chapter 3 - Modeling components and overview*. Version Final (p. 72). Coastal Protection and Restoration Authority.

Cahoon, D. R., Hensel, P. F., Spencer, T., Reed, D. J., McKee, K. L., & Saintilan, N. (2006). Coastal wetland vulnerability to relative sea-level rise: Wetland elevation trends and process controls. In J. T. A. Verhoeven, B. Beltman, R. Bobbink, & D. F. Whigham (Eds.), *Wetlands and natural resource management*, *Ecological studies* (Vol. 190, pp. 271–292). Springer Berlin Heidelberg. https://doi.org/10.1007/978-3-540-33187-2_12

Callaway, J. C., Nyman, J. A., & DeLaune, R. D. (1996). Sediment accretion in coastal wetlands: A review and a simulation model of processes. In *Current topics in wetland biogeochemistry* (Vol. 2, (No. 2), p. 23).

Chenevert, E. (2023). EChenevert/for_paper2023: Vertical accretion in Louisiana study (v.1). *Zenodo*. https://doi.org/10.5281/zenodo.10396266

Coastal Protection and Restoration Authority (CPRA) of Louisiana. (2023). *Coastwide reference monitoring system*. Coastal Information Management System (CIMS) Database. Retrieved from https://cims.coastal.la.gov

Coleman, D. J., Schuerch, M., Temmerman, S., Guntenspergen, G., Smith, C. G., & Kirwan, M. L. (2022). Reconciling models and measurements of marsh vulnerability to sea level rise. *Limnology & Oceanography Letters*, *7*(2), 140–149. https://doi.org/10.1002/lol2.10230

Coleman, J. M. (1988). Dynamic changes and processes in the Mississippi River delta. *Geological Society of America Bulletin*, *100*(7), 999–1015. https://doi.org/10.1130/0016-7606(1988)100<0999:DCAPIT>2.3.CO;2

Cormier, N., Krauss, K. W., & Conner, W. H. (2013). Periodicity in stem growth and litterfall in tidal freshwater forested wetlands: Influence of salinity and drought on nitrogen recycling. *Estuaries and Coasts*, *36*(3), 533–546. https://doi.org/10.1007/s12237-012-9505-z

Cortese, L., & Fagherazzi, S. (2022). Fetch and distance from the bay control accretion and erosion patterns in Terrebonne marshes (Louisiana, USA). *Earth Surface Processes and Landforms*, *47*(6), 1455–1465. https://doi.org/10.1002/esp.5327

Cortese, L., Jensen, D. J., Simard, M., & Fagherazzi, S. (2023). Using normalize difference vegetation index to infer wetlands salinity and organic contribution to vertical accretion rates. *Journal of Geophysical Research: Biogeosciences*, *128*(11), e2023JG007631. https://doi.org/10.1029/2023JG007631

Couvillion, B. R., Barras, J. A., Steyer, G. D., Sleavin, W., Fischer, M., Beck, H., et al. (2011). Land area change in coastal Louisiana from 1932 to 2010. U.S. Geological Survey Scientific Investigations Map 3164, scale 1:265,000, 12 p. pamphlet.

Couvillion, B. R., Beck, H., Schoolmaster, D., & Fischer, M. (2017). *Land area change in coastal Louisiana (1932 to 2016)*. Report. Scientific Investigations Map. USGS Publications Warehouse. https://doi.org/10.3133/sim3381

Curcó, A., Ibàñez, C., Day, J. W., & Prat, N. (2002). Net primary production and decomposition of salt marshes of the Ebre Delta (Catalonia, Spain). *Estuaries*, *25*(3), 309–324. https://doi.org/10.1007/BF02695976

Day, J., Clark, H., Chang, C., Hunter, R., & Norman, C. (2020). Life cycle of oil and gas fields in the Mississippi River Delta: A review. *Water*, *12*(5), 1492. https://doi.org/10.3390/w12051492

Edmonds, D. A., Toby, S. C., Siverd, C. G., Twilley, R., Bentley, S. J., Hagen, S., & Xu, K. (2023). Land loss due to human-altered sediment budget in the Mississippi River Delta. *Nature Sustainability*, *6*(6), 644–651. https://doi.org/10.1038/s41893-023-01081-0

Ensign, S. H., Hupp, C. R., Noe, G. B., Krauss, K. W., & Stagg, C. L. (2014). Sediment accretion in tidal freshwater forests and oligohaline marshes of the Waccamaw and Savannah Rivers, USA. *Estuaries and Coasts*, *37*(5), 1107–1119. https://doi.org/10.1007/s12237-013-9744-7

Evers, D. E., Sasser, C. E., Gosselink, J. G., Fuller, D. A., & Visser, J. M. (1998). The impact of vertebrate herbivores on wetland vegetation in Atchafalaya Bay, Louisiana. *Estuaries*, *21*(1), 1. https://doi.org/10.2307/1352543

Falcini, F., Khan, N. S., Macelloni, L., Horton, B. P., Lutken, C. B., McKee, K. L., et al. (2012). Linking the historic 2011 Mississippi River flood to coastal wetland sedimentation. *Nature Geoscience*, *5*(11), 803–807. https://doi.org/10.1038/ngeo1615

Global Wind Atlas. (2022). *Global Wind Atlas 3.0, a free, web-based application developed, owned and operated by the Technical University of Denmark (DTU)*. The Global Wind Atlas 3.

Han, J., & Kamber, M. (2012). *Data mining: Concepts and techniques* (3rd ed.). Elsevier.

Hayes, M. P., Yadav Sapkota, J. R. W., & Cook, R. L. (2021). Investigating the impact of in situ soil organic matter degradation through porewater spectroscopic analyses on marsh edge erosion. *Chemosphere*, *268*, 129266. https://doi.org/10.1016/j.chemosphere.2020.129266

Hiatt, M., Gregg, S., Day, J. W., Rohli, R. V., Andrew Nyman, J., Lane, R., & Sharp, L. A. (2019). Drivers and impacts of water level fluctuations in the Mississippi River Delta: Implications for delta restoration. *Estuarine, Coastal and Shelf Science*, *224*, 117–137. https://doi.org/10.1016/j.ecss.2019.04.020

Hopkinson, C. S., Morris, J. T., Fagherazzi, S., Wollheim, W. M., & Raymond, P. A. (2018). Lateral marsh edge erosion as a source of sediments for vertical marsh accretion. *Journal of Geophysical Research: Biogeosciences*, *123*(8), 2444–2465. https://doi.org/10.1029/2017JG004358

Howes, N. C., FitzGerald, D. M., Hughes, Z. J., Georgiou, I. Y., Kulp, M. A., Miner, M. D., et al. (2010). Hurricane-induced failure of low salinity wetlands. *Proceedings of the National Academy of Sciences*, *107*(32), 14014–14019. https://doi.org/10.1073/pnas.0914582107

Jankowski, K. L., Törnqvist, T. E., & Fernandes, A. M. (2017). Vulnerability of Louisiana's coastal wetlands to present-day rates of relative sea-level rise. *Nature Communications*, *8*(1), 14792. https://doi.org/10.1038/ncomms14792

Janousek, C. N., & Mayo, C. (2013). Plant responses to increased inundation and salt exposure: Interactive effects on tidal marsh productivity. *Plant Ecology*, *214*(7), 917–928. https://doi.org/10.1007/s11258-013-0218-6

Jarvis, J. C. (2010). *Vertical accretion rates in coastal Louisiana: A review of the scientific literature*. ERDC/EL TN-10-5 (p. 15). U.S. Army Engineer Research and Development Center.

Jensen, D. J., Cavanaugh, K. C., Thompson, D. R., Fagherazzi, S., Cortese, L., & Simard, M. (2022). Leveraging the historical Landsat catalog for a remote sensing model of wetland accretion in coastal Louisiana. *Journal of Geophysical Research: Biogeosciences*, *127*(6), e2022JG006794. https://doi.org/10.1029/2022JG006794

Kearney, M. S., Stutzer, D., Kevin, T., & Stevenson, J. C. (2009). The effects of tidal inundation on the reflectance characteristics of coastal marsh vegetation. *Journal of Coastal Research*, *256*, 1177–1186. https://doi.org/10.2112/08-1080.1

Keogh, M. E., Kolker, A. S., Snedden, G. A., & Renfro, A. A. (2019). Hydrodynamic controls on sediment retention in an emerging diversion-fed delta. *Geomorphology*, *332*, 100–111. https://doi.org/10.1016/j.geomorph.2019.02.008

Keogh, M. E., Törnqvist, T. E., Kolker, A. S., Erkens, G., & Bridgeman, J. G. (2021). Organic matter accretion, shallow subsidence, and river delta sustainability. *Journal of Geophysical Research: Earth Surface*, *126*(12), e2021JF006231. https://doi.org/10.1029/2021JF006231

Kirwan, M. L., & Guntenspergen, G. R. (2012). Feedbacks between inundation, root production, and shoot growth in a rapidly submerging brackish marsh: Marsh root growth under sea level rise. *Journal of Ecology*, *100*(3), 764–770. https://doi.org/10.1111/j.1365-2745.2012.01957.x

Kolker, A. S., Allison, M. A., & Sultan, H. (2011). An evaluation of subsidence rates and sea-level variability in the northern Gulf of Mexico: Subsidence and sea level variability. *Geophysical Research Letters*, *38*(21), n/a. https://doi.org/10.1029/2011GL049458

Lamb, M. P., & Mohrig, D. (2009). Do hyperpycnal-flow deposits record river-flood dynamics? *Geology*, *37*(12), 1067–1070. https://doi.org/10.1130/G30286A.1

Lane, R. R., Reed, D. J., Day, J. W., Kemp, G. P., McDade, E. C., & Rudolf, W. B. (2020). Elevation and accretion dynamics at historical plots in the Biloxi Marshes, Mississippi Delta. *Estuarine, Coastal and Shelf Science*, *245*, 106970. https://doi.org/10.1016/j.ecss.2020.106970

Lundberg, S., & Lee, S.-I. (2017). A unified approach to interpreting model predictions. https://doi.org/10.48550/ARXIV.1705.07874

Mariotti, G., & Carr, J. (2014). Dual role of salt marsh retreat: Long-term loss and short-term resilience. *Water Resources Research*, *50*(4), 2963–2974. https://doi.org/10.1002/2013WR014676

Mariotti, G., Elsey-Quirk, T., Bruno, G., & Valentine, K. (2020). Mud-associated organic matter and its direct and indirect role in marsh organic matter accumulation and vertical accretion. *Limnology & Oceanography*, *65*(11), 2627–2641. https://doi.org/10.1002/lno.11475

McKee, K. L. (2011). Biophysical controls on accretion and elevation change in Caribbean mangrove ecosystems. *Estuarine, Coastal and Shelf Science*, *91*(4), 475–483. https://doi.org/10.1016/j.ecss.2010.05.001

Meade, R. H., & Moody, J. A. (2009). Causes for the decline of suspended-sediment discharge in the Mississippi River System, 1940-2007. *Hydrological Processes*, *24*(1), 35–49. https://doi.org/10.1002/hyp.7477

Miller, R. L., & McKee, B. A. (2004). Using MODIS Terra 250 m imagery to map concentrations of total suspended matter in coastal waters. *Remote Sensing of Environment*, *93*(1–2), 259–266. https://doi.org/10.1016/j.rse.2004.07.012

Mo, Y., Kearney, M., & Momen, B. (2017). Drought-associated phenological changes of coastal marshes in Louisiana. *Ecosphere*, *8*(5), e01811. https://doi.org/10.1002/ecs2.1811

Molnar, C. (2019). Interpretable machine learning: A guide for making black box models explainable.

Mudd, S. M., D'Alpaos, A., & Morris, J. T. (2010). How does vegetation affect sedimentation on tidal marshes? Investigating particle capture and hydrodynamic controls on biologically mediated sedimentation. *Journal of Geophysical Research*, *115*(F3), F03029. https://doi.org/10.1029/2009JF001566

Nardin, W., & Edmonds, D. A. (2014). Optimum vegetation height and density for inorganic sedimentation in deltaic marshes. *Nature Geoscience*, *7*(10), 722–726. https://doi.org/10.1038/ngeo2233

Narron, C. R., O'Connell, J. L., Mishra, D. R., Cotten, D. L., Hawman, P. A., & Mao, L. (2022). Flooding in Landsat across Tidal Systems (FLATS): An index for intermittent tidal filtering and frequency detection in salt marsh environments. *Ecological Indicators*, *141*, 109045. https://doi.org/10.1016/j.ecolind.2022.109045

Nienhuis, J. H., Törnqvist, T. E., Jankowski, K. L., Fernandes, A. M., & Keogh, M. E. (2017). A new subsidence map for coastal Louisiana. *Geological Society of America Today*, 60–61. https://doi.org/10.1130/GSATG337GW.1

Nyman, J. A., DeLaune, R. D., Pezeshki, S. R., & Patrick, W. H. (1995). Organic matter fluxes and marsh stability in a rapidly submerging estuarine marsh. *Estuaries*, *18*(1), 207. https://doi.org/10.2307/1352631

Nyman, J. A., Walters, R. J., Delaune, R. D., & Patrick, W. H., Jr. (2006). Marsh vertical accretion via vegetative growth. *Estuarine, Coastal and Shelf Science*, *69*(3–4), 370–380. https://doi.org/10.1016/j.ecss.2006.05.041

Pekel, J.-F., Cottam, A., Gorelick, N., & AlanBelward, S. (2016). High-resolution mapping of global surface water and its long-term changes. *Nature*, *540*(7633), 418–422. https://doi.org/10.1038/nature20584

Rasmussen, C. E., & Williams, C. K. I. (2005). *Gaussian processes for machine learning*. The MIT Press. https://doi.org/10.7551/mitpress/3206.001.0001

Reddy, K. R., & DeLaune, R. D. (2008). *Biogeochemistry of wetlands: Science and applications*. CRC Press.

Roy, S., Robeson, S. M., Ortiz, A. C., & Edmonds, D. A. (2020). Spatial and temporal patterns of land loss in the Lower Mississippi River Delta from 1983 to 2016. *Remote Sensing of Environment*, *250*, 112046. https://doi.org/10.1016/j.rse.2020.112046

Sanks, K. M., Shaw, J. B., & Naithani, K. (2020). Field-based estimate of the sediment deficit in coastal Louisiana. *Journal of Geophysical Research: Earth Surface*, *125*(8), e2019JF005389. https://doi.org/10.1029/2019JF005389

Shen, Z., Törnqvist, T. E., Mauz, B., Chamberlain, E. L., Nijhuis, A. G., & Sandoval, L. (2015). Episodic overbank deposition as a dominant mechanism of floodplain and delta-plain aggradation. *Geology*, *43*(10), 875–878. https://doi.org/10.1130/G36847.1

Silva, S. J., Keller, C. A., & Hardin, J. (2022). Using an explainable machine learning approach to characterize earth system model errors: Application of SHAP analysis to modeling lightning flash occurrence. *Journal of Advances in Modeling Earth Systems*, *14*(4), e2021MS002881. https://doi.org/10.1029/2021MS002881

Smith, J. E., Bentley, S. J., Snedden, G. A., & White, C. (2015). What role do hurricanes play in sediment delivery to subsiding river deltas? *Scientific Reports*, *5*(1), 17582. https://doi.org/10.1038/srep17582

Solohin, E., Widney, S. E., & Craft, C. B. (2020). Declines in plant productivity drive loss of soil elevation in a tidal freshwater marsh exposed to saltwater intrusion. *Ecology*, *101*(12), e03148. https://doi.org/10.1002/ecy.3148

Stagg, C. L., Baustian, M. M., Perry, C. L., Carruthers, T. J. B., & Hall, C. T. (2018). "Direct and indirect controls on organic matter decomposition in four coastal wetland communities along a landscape salinity gradient." Edited by Amy Zanne. *Journal of Ecology*, *106*(2), 655–670. https://doi.org/10.1111/1365-2745.12901

Steyer, G. D. (2010). *Coastwide reference monitoring system (CRMS)*. Report. Fact Sheet. USGS Publications Warehouse. https://doi.org/10.3133/fs20103018

Steyer, G. D., Sasser, C. E., Visser, J. M., Swenson, E. M., Nyman, J. A., & Raynie, R. C. (2003). A proposed coast-wide reference monitoring system for evaluating wetland restoration trajectories in Louisiana. *Environmental Monitoring and Assessment*, *81*(1/3), 107–117. https://doi.org/10.1023/A:1021368722681

Suir, G. M., & Sasser, C. E. (2019). Use of NDVI and landscape metrics to assess effects of riverine inputs on wetland productivity and stability. *Wetlands*, *39*(4), 815–830. https://doi.org/10.1007/s13157-019-01132-3

Sun, C., Fagherazzi, S., & Liu, Y. (2018). Classification mapping of salt marsh vegetation by flexible monthly NDVI time-series using landsat imagery. *Estuarine, Coastal and Shelf Science*, *213*, 61–80. https://doi.org/10.1016/j.ecss.2018.08.007

Thorne, K., Scott, J., Freeman, C., Kevin, B., Janousek, C., & Guntenspergen, G. (2022). Atmospheric river storm flooding influences tidal marsh elevation building processes. *Journal of Geophysical Research: Biogeosciences*, *127*(3), e2021JG006592. https://doi.org/10.1029/2021JG006592

Törnqvist, T. E., Paola, C., Parker, G., Liu, K.-B., Mohrig, D., Holbrook, J. M., & Twilley, R. R. (2007). Comment on 'Wetland sedimentation from hurricanes Katrina and Rita'. *Science*, *316*(5822), 201. https://doi.org/10.1126/science.1136780

Turner, R. E., Baustian, J. J., Swenson, E. M., & Spicer, J. S. (2006). Wetland sedimentation from hurricanes Katrina and Rita. *Science*, *314*(5798), 449–452. https://doi.org/10.1126/science.1129116

Turner, R. E., Swenson, E. M., & Milan, C. S. (2002). Organic and inorganic contributions to vertical accretion in salt marsh sediments. In M. P. Weinstein & D. A. Kreeger (Eds.), *Concepts and controversies in tidal marsh ecology* (pp. 583–595). Kluwer Academic Publishers. https://doi.org/10.1007/0-306-47534-0_27

Turner, R. E., Swenson, E. M., Milan, C. S., Lee, J. M., & Oswald, T. A. (2004). Below-ground biomass in healthy and impaired salt marshes: Salt marsh resilience below-ground. *Ecological Research*, *19*(1), 29–35. https://doi.org/10.1111/j.1440-1703.2003.00610.x

Tweel, A. W., & Turner, R. E. (2012). Watershed land use and river engineering drive wetland formation and loss in the Mississippi River Birdfoot Delta. *Limnology & Oceanography*, *57*(1), 18–28. https://doi.org/10.4319/lo.2012.57.1.0018

Twilley, R. R., Day, J. W., Bevington, A. E., Castañeda-Moya, E., Christensen, A., Holm, G., et al. (2019). Ecogeomorphology of coastal deltaic floodplains and estuaries in an active delta: Insights from the Atchafalaya Coastal Basin. *Estuarine, Coastal and Shelf Science*, *227*, 106341. https://doi.org/10.1016/j.ecss.2019.106341

Visser, J. M., Sasser, C. E., Chabreck, R. H., & Greg Linscombe, R. (2002). The impact of a severe drought on the vegetation of a subtropical estuary. *Estuaries*, *25*(6), 1184–1195. https://doi.org/10.1007/BF02692215

Visser, J. M., Sasser, C. E., Chabreck, R. H., & Linscombe, R. G. (1999). Long-term vegetation change in Louisiana tidal marshes, 1968–1992. *Wetlands*, *19*(1), 168–175. https://doi.org/10.1007/BF03161746

Wager, R. T., & Haywood, E. L., III. (2022). State of Louisiana Coastal Protection and Restoration Authority (CPRA) Coastal Information Management System (CIMS) data dictionary. Version 1.0 (pp. 1–133).

Weston, N. B., Vile, M. A., Neubauer, S. C., & Velinsky, D. J. (2011). Accelerated microbial organic matter mineralization following salt-water intrusion into tidal freshwater marsh soils. *Biogeochemistry*, *102*(1–3), 135–151. https://doi.org/10.1007/s10533-010-9427-4

White, E. D., Reed, D. J., & Meselhe, E. A. (2019). Modeled sediment availability, deposition, and decadal land change in coastal Louisiana marshes under future relative sea level rise scenarios. *Wetlands*, *39*(6), 1233–1248. https://doi.org/10.1007/s13157-019-01151-0

Williams, E. K., & Rosenheim, B. E. (2015). What happens to soil organic carbon as coastal marsh ecosystems change in response to increasing salinity? An exploration using ramped pyrolysis: Fate of coastal SOC with salinity. *Geochemistry, Geophysics, Geosystems*, *16*(7), 2322–2335. https://doi.org/10.1002/2015GC005839

Xu, K., Bentley, S. J., Day, J. W., & Freeman, A. M. (2019). A review of sediment diversion in the Mississippi River Deltaic plain. *Estuarine, Coastal and Shelf Science*, *225*, 106241. https://doi.org/10.1016/j.ecss.2019.05.023

Xu, Y., Esposito, C. R., Beltrán-Burgos, M., & HeidiNepf, M. (2022). Competing effects of vegetation density on sedimentation in deltaic marshes. *Nature Communications*, *13*(1), 4641. https://doi.org/10.1038/s41467-022-32270-8